NASA TECHNICAL REPORT

RADIATIVE HEAT TRANSFER BETWEEN PLANAR SURFACES WITH FILLETED JUNCTURES

by Wm. Prichard Jones

Ames Research Center

Moffett Field, Calif.

RADIATIVE HEAT TRANSFER BETWEEN PLANAR SURFACES

WITH FILLETED JUNCTURES

By Wm. Prichard Jones

Ames Research Center
Moffett Field, Calif.

NATIONAL AERONAUTICS AND SPACE ADMINISTRATION

TECHNICAL REPORT R-157

RADIATIVE HEAT TRANSFER BETWEEN PLANAR SURFACES

WITH FILLETED JUNCTURES

By Wm. Prichard Jones

SUMMARY

21255

A numerical analysis of the effect of a circular fillet on the thermal
radiation exchange between planar surfaces of zero conductivity intersecting at a
sharp angle is presented. Temperature variation along the surface for a constant
heat transfer and local heat-transfer variation for a constant wall temperature
is obtained. Surface emissivity, which is assumed to be independent of wavelength
and temperature, and fillet size are varied in the analysis. The "hot spot" for
the unfilleted structure is found at the intersection of the planar surfaces but
is moved to the point of juncture in the case of a filleted structure and is
reduced in value. For planar surfaces that intersect at a right angle, the temper-
ature and local heat-transfer distributions for various fillet sizes are compared
with the corresponding distributions of the unfilleted surface. Exact results are
compared also with the temperature and heat-transfer distributions obtained from
an approximation to the radiation flux function which is based on the use of a
shape factor. For a wide range of values for the emissivity and fillet size, the
agreement between approximate and exact results is within 5 percent. Author

INTRODUCTION

Interest in radiative cooling of space vehicles, solar energy collectors,
and thermal radiation shields has brought about a need to increase the fund of
engineering knowledge through predictions of the characteristics of basic geometric
configurations and through application of available mathematical techniques to the
analysis of the fundamental equations. Heaslet and Lomax contributed to that fund
by examining the radiative heat transfer between conducting planar surfaces that
intersect at a sharp angle (ref. 1). These same authors also studied the radia-
tive heat transfer for infinite, nonconducting shells with circular-arc sections
(ref. 2). The purpose of this paper is to extend the results of these two recently
published analyses by wedding the two configurations employed in their work. Thus,
planar surfaces are joined by a concave surface of arbitrary radius, that is,
joined by a fillet. The presence of the fillet at the juncture of the planar sur-
faces affects the magnitude and distribution of radiation flux, exact solutions
for which are obtained from a machine code that incorporates the Liouville-Neumann

method of solving a Fredholm integral equation of the second kind. Simple, closed-form solutions for certain limiting conditions provide a partial check on numerical results.

The emphasis in this analysis will be placed on, first, the influence of the fillet on the radiative flux distribution corresponding to the unfilleted structure and, second, the importance of surface emissivity. Effects of thermal conduction will not be treated here, thus eliminating nonlinear terms in the governing integral equation. The configuration, two-dimensional surfaces intersecting at right angles, suffices to illustrate the alteration of the flux distribution due to changes in the primary parameter, fillet size. As in references 1 and 2, the surface properties of absorptivity and reflectivity are assumed to be independent of surface temperature, and wavelength of radiation. The emissivity of the surface is assumed equal to the absorptivity, less than unity and constant at all temperatures and at all wavelengths. By definition, then, the surface is gray. In addition, it is assumed that emission and reflection are diffuse and only the concave side of the configuration radiates.

Two physical problems are formulated and solved for a filleted structure. In the first example the surface is held at a constant temperature and the variation in local heat transfer along the surface is found. In the second example a constant heat transfer is provided and the variation in temperature along the surface is found. The solutions to these problems are compared with corresponding solutions for an unfilleted structure (some of which do not appear in ref. 1) to demonstrate the influence of the fillet.

To compare solutions corresponding to different fillet sizes, the total length of the combined surfaces is held constant. Fillet size, therefore, can be given simply as the ratio of fillet length to total length. When this ratio is 1, the present results for local heat transfer and temperature variation are identical with results published in reference 2, which treats radiative transfer for infinite shells with circular-arc sections. For a length ratio of 0 the local heat-transfer solution without conduction is the same as that given in reference 1, but the second example, temperature variation with constant heat transfer for adjoining plates, is given here.

NOTATION

a   see figure 1

B(s)   total radiation flux function (energy per unit area, time)

c   distance between field and source points

f(s)   shape factor defined in equation (31)

G(s)   unknown function in equation (12)

H(s)   flux of incident radiation defined in equation (3)

K(s, s')   kernel function defined in equation (1)

l dimensionless length of straight-line segment on surface

L   length of straight-line segment on surface cross section

L_T total length of surface cross section, 2S + 2L

Q(s)   local heat-transfer function defined in equation (7)

r   dimensionless radius of fillet, $\dfrac{R}{S + L}$

r_s ratio of total fillet arc length to total surface length, $\dfrac{S}{S + L}$

R   radius of circular arc

s   surface coordinate of point divided by S + L

S   half-length of circular-arc segment on surface cross section, $\dfrac{\pi R}{4}$

T(s)   temperature function

x   Cartesian coordinate divided by S + L

y   Cartesian coordinate divided by S + L

α absorptivity of gray surface

β slope angle of surface at field point, arc tan $\dfrac{dy}{dx}$

δ difference in left and right value of derivative of a function

ϵ emissivity of gray surface

θ angular coordinate of point on surface

Θ_O scale constant determined by equation (18) when evaluated at s = 0

λ parameter defined by equation (13) or (14)

ρ reflectivity of gray surface

φ angle measured from normal to surface at field point to line joining field and source points, arc sin $\dfrac{a}{c}$ (counterclockwise, +; clockwise, -)

3

Subscripts

o   constant value of function

R   maximum value of function used as reference value

1   approximate value of a function

Superscripts

'   source of radiation; unprimed coordinate refers to location of field point, that is, coordinate of receiver

FORMULATION OF PROBLEM

Consider a concave cylindrical surface of infinite width, a cross section of which is shown in figure 1, that is symmetric about a generatrix of the surface midway between the ends. Length along a cross section of the surface is measured from the midline and in a direction perpendicular to the generators of the surface. The characteristic dimension for this problem is the half-length, $L_T/2$, of the surface cross section and it is used to make all quantities involving length dimensionless. Since the surface is two-dimensional, an infinitesimal element of area of unit width is represented by ds or ds' where s' is the dimensionless surface coordinate that locates the source line element and s locates the field line element at which radiation is incident.

The thermal radiation field (energy/unit time) incident at a field point, s, lying on the concave side of the surface is calculated by summing the total radiation emitted at all source points, s', also lying on the concave side of the surface. Diffusely radiating elements are assumed to satisfy Lambert's cosine law. This means that when the normals to the elements, ds and ds', at the field point and source point, respectively, are projected onto the line joining the points, the flux received by each element is directly proportional to the area of the projected elements. In the idealized problem to be treated here, the normals, N and N', are coplanar, affording a simple expression for the angle factor (see ref. 3).

$$\frac{1}{2} \left| \sin \varphi(s, s') \right|$$

The _incremental_ angle factor, or kernel function times the source element, ds', determines the fraction of energy emitted and reflected at ds' that falls directly on ds and is given as

$$\frac{1}{2} \left| d(\sin \varphi) \right| = K(s, s')ds' \tag{1}$$

4

where φ is the angle measured (counterclockwise, +: clockwise, -) from the normal to the surface at the field point to the line joining the source and field points. Equation (1) defines the kernel function, $K(s, s')$. The mathematical form and properties of the kernel that are pertinent to the present problem, apart from the matter of machine coding, will be set forth in the next section.

Each element of the surface emits radiation according to the Stefan-Boltzmann law adjusted by a factor, ϵ, the emissivity of the surface. An energy-flux balance for an element ds' on the concave side of the surface is written as a sum of two terms: the emitted radiation, $\epsilon\sigma T^4(s')$, and the reflected radiation, $\rho H(s')$, where $H(s')$ is the energy-flux incident at s' and ρ is the reflectivity of the surface. The total flux, $B(s')$, ensuing from the source point is

$$B(s') = \epsilon\sigma T^4(s') + \rho H(s') \tag{2}$$

where the function $H(s')$ is

$$H(s') = \int_{L_T} B(s)K(s, s')ds \tag{3}$$

an integral of the total flux arriving at s' summed over the entire length of the surface. The source and field points are interchangeable, so that the integral equation for the total flux leaving ds is

$$B(s) = \epsilon\sigma T^4(s) + \rho \int_{L_T} B(s')K(s, s')ds' \tag{4}$$

For the gray surface considered here the coefficients of reflectivity, ρ, absorptivity, α, and emissivity, ϵ, satisfy the relations

$$1 = \rho + \alpha \tag{5}$$

$$\epsilon = \alpha \tag{6}$$

The latter equation is Kirchhoff's law under the condition of temperature equilibrium. The heat-transfer function is defined as

$$Q(s) = B(s) - H(s) \tag{7}$$

which, combined with equations (2), (5), and (6), gives

$$B(s) = \sigma T^4(s) - \frac{1 - \epsilon}{\epsilon} Q(s) \tag{8}$$

5

Inserting equation (8) into (4) casts the inhomogeneous integral equation (4) into a form convenient to formulate the two problems mentioned earlier. The basic equation which serves as a starting point for the numerical work is

$$\epsilon\sigma T^4(s) - Q(s) = \int_{L_T} \left[\epsilon\sigma T^4(s') - \rho Q(s')\right] K(s, s')ds' \tag{9}$$

and the two problems are stated next in dimensionless form.

If a constant temperature, T_O, is maintained everywhere on the surface, then equation (9) becomes

$$\frac{Q(s)}{\sigma T_O{}^4} = \epsilon + (1 - \epsilon) \int_{L_T} \left[\frac{Q(s')}{\sigma T_O{}^4} - \frac{\epsilon}{1 - \epsilon}\right] K(s, s')ds' \tag{10}$$

If, instead, a constant heat transfer, Q_O, is provided everywhere, then equation (9) takes the form

$$\frac{\sigma T^4(s)}{Q_O} = \frac{1}{\epsilon} + \int_{L_T} \left[\frac{\sigma T^4(s')}{Q_O} - \frac{1 - \epsilon}{\epsilon}\right] K(s, s')ds' \tag{11}$$

In the formal mathematical solution of equation (10) or (11) or both, one considers the Fredholm integral equation

$$G(s) = 1 + \lambda \int_{L_T} G(s')K(s, s')ds' \tag{12}$$

where, for the constant temperature case,

$$\left.\begin{array}{l} G(s) = \dfrac{1}{\epsilon} - \dfrac{1 - \epsilon}{\epsilon^2} \dfrac{Q(s)}{\sigma T_O{}^4} \\[2em] \lambda = 1 - \epsilon \end{array}\right\} \tag{13}$$

and in the case of constant heat transfer

$$\left.\begin{array}{l} G(s) = \dfrac{\sigma T^4(s)}{Q_O} - \dfrac{1 - \epsilon}{\epsilon} \\[2em] \lambda = 1 \end{array}\right\} \tag{14}$$

6

It can be seen from equations (12) and (14) that the gradient of the temperature field is independent of the emissivity, whereas the gradient of the heat-transfer field is altered by the presence of the factor $(1 - \epsilon)/\epsilon^2$ in equation (13).

Equations (10) and (11), or equivalently, equation (12) with (13) or (14), are solved numerically for the configuration shown in figure 2. It consists of planes of length L whose extensions intersect at right angles which are joined by a concave surface of length 2S, a section of which is a circular arc. The parameter, r_s, is defined as

$$r_s = \frac{S}{S + L} \tag{15}$$

and will be varied in the analysis along with the emissivity. In order to compare different configurations, the total length of the surface, L_T, where

$$L_T = 2S + 2L \tag{16}$$

is held constant. Since dimensions involving length have been made dimensionless by dividing by the surface half-length, $L_T/2$, the limits of integration in the surface coordinate system become +1 and -1.

Before examination of the composite kernel function in the next section, it is noted that equations (10) and (11) have a simple analytic form in the special case that

$$r_s = 1$$

that is, when the plane surface length, L, is zero. The configuration then is an infinite shell with a circular-arc section for which the solutions to the two problems stated above are given in reference 2. They are

$$\frac{Q(s)}{\sigma T_o{}^4} = \epsilon \left(\cos \sqrt{\epsilon} \, \frac{\pi}{8} + \sqrt{\epsilon} \, \tan \frac{\pi}{8} \cos \sqrt{\epsilon} \, \frac{\pi}{8} \right)^{-1} \cos \left(\sqrt{\epsilon} \, \frac{\pi}{8} \, s \right) \tag{17}$$

for the constant shell temperature and

$$\frac{\sigma T^4(s)}{Q_o} = \frac{1}{\epsilon} + \frac{\pi}{8} \tan \frac{\pi}{8} + \frac{1}{2} \left[\left(\frac{\pi s}{8} \right)^2 - \left(\frac{\pi}{8} \right)^2 \right] \tag{18}$$

for the uniform heat transfer. The symbol R, the radius of the circular arc, is related to the fillet parameter, r_s, by the expression

$$R = \frac{2 r_s L_T}{\pi} \tag{19}$$

From this identity the angular coordinate, θ, employed in reference 2 and equations (17) and (18) here, is related to the surface coordinate and fillet parameter by

$$\theta = \frac{\pi}{4} \frac{s}{r_s} \tag{20}$$

for $|s| \leq r_s$.

Exact solutions to equations (10) and (11) are obtained from equations (12), (13), and (14) with the aid of a Fortran program for the IBM 7090.

KERNEL FUNCTION

The kernel function that appears in the integral equation governing the radiation flux function is defined as the absolute value of the gradient of the angle factor. For any two-dimensional, continuous configuration with piecewise continuous curvature, the angle factor is

$$|\sin \varphi(x, y; x', y')| = \frac{|(x - x') \cos \beta + (y - y') \sin \beta|}{\sqrt{(x - x')^2 + (y - y')^2}} \tag{21}$$

where $\beta = \arctan dy/dx$. A transformation from Cartesian coordinates to surface coordinates (see fig. 2) is convenient when dealing with a composite surface. For three choices of location of field and source points, equation (21) assumes a compact form. For example, when both points lie on the circular arc, the angle factor is

$$\frac{1}{2} \cos \frac{\pi}{8r_s} |s - s'|$$

and is employed in reference 2. When both points lie together on either straight-line segment, the angle factor is unity; whereas if the field point is on one straight part and the source point is on the other which is the case considered in reference 1, the angle factor (eq. (21)) can be written as

$$\frac{\pi}{8r_s} \frac{1 + \frac{\pi}{4}\left(\frac{s}{r_s} - 1\right)}{\sqrt{\left[1 + \frac{\pi}{4}\left(\frac{s}{r_s} - 1\right)\right]^2 + \left[1 + \frac{\pi}{4}\left(-\frac{s'}{r_s} - 1\right)\right]^2}}$$

8

The different forms of the kernel function corresponding to the three angle factors enumerated above as well as the angle factors which result from the other possible locations of field and source points are computed using equation (1) and are listed in figure 3. A perspective drawing, figure 4, depicts the approximate behavior of $K(s, s')$ for $r_s = 0.3$ and exposes a property of the composite kernel function that is an aid to checking the final numerical results. It is evident that the gradient of $K(s, s')$ is discountinuous at several places. At the juncture of the concave and plane surface, the radius of curvature jumps discontinuously from a finite value to infinity. Hence, the derivative of the kernel is discontinuous at the juncture also, namely, at $s' = r_s$ and $s = r_s$. (It is also discontinuous at $s = s'$.)

The discontinuity in the kernel gradient causes a break in the slope of the curves that represent $Q(s)/\sigma T_0{}^4$ and $\sigma T^4(s)/Q_0$ at $s = r_s$. At the juncture point the derivative of either function takes on two values which are determined accordingly as $s = r_s$ is approached from the left or from the right. The slope difference formula for each function can be found, first, by writing down the total radiation flux, $B(s)$, as seen from points on either side and very close to the juncture, then by differentiating with respect to the field coordinate, s, and finally, by passing to the limit, r_s. Thus, let s_1 and s_2 be points to the left and to the right of r_s and very close to it. The difference in slope of the functions, $Q(s)/T_0{}^4$ and $T^4(s)/Q_0$, can be obtained most simply from the dimensionless, canonical form of the basic integral equation, (12), with equations (13) and (14), in the place of the dimensional flux function $B(s)$ mentioned above. Expressions for $G(s)$ to the left and right of r_s are

$$G(s_1) = 1 + \lambda \left[\int_{-1}^{-r_s} G(s')K_{IV}{}^*(s_1, s')ds' + \int_{-r_s}^{s_1} G(s')K_I(s_1, s')ds' \right.$$

$$\left. + \int_{s_1}^{r_s} G(s')K_I(s_1, s')ds' + \int_{r_s}^{1} G(s')K_{IV}(s_1, s')ds' \right] \qquad (22)$$

and

$$G(s_2) = 1 + \lambda \left[\int_{-1}^{-r_s} G(s')K_{III}{}^*(s_2, s')ds' + \int_{-r_s}^{r_s} G(s')K_{II}(s_2, s')ds' \right.$$

$$\left. + \int_{r_s}^{1} G(s')K_{III}(s_2, s')ds' \right] \qquad (23)$$

The slope difference formula for $G(r_s)$ is

$$\delta \left. \frac{\partial G(s)}{\partial s} \right|_{s=r_s} = \lim_{s_1 \to r_s} \frac{\partial G(s_1)}{\partial s_1} - \lim_{s_2 \to r_s} \frac{\partial G(s_2)}{\partial s_2} \qquad (24)$$

9

and when equation (24) is combined with (22) and (23), the final form is written compactly as

$$\delta \left.\frac{\partial G(s)}{\partial s}\right|_{s=r_s} = \lambda\left[\int_{-1}^{-r_s} G(s')\left(\frac{\partial K_{IV}*}{\partial s} - \frac{\partial K_{III}*}{\partial s}\right)ds'\right.$$

$$\left. + \int_{-r_s}^{r_s} G(s')\left(\frac{\partial K_I}{\partial s} - \frac{\partial K_{II}}{\partial s}\right)ds' + \int_{r_s}^{1} G(s')\frac{\partial K_{IV}}{\partial s}ds'\right] \tag{25}$$

Expressions for $K(s, s')$ are given in figure 3.

As can be seen from figure 4 the composite kernel function itself is continuous, is never negative, and is bounded everywhere except in the limit as r_s goes to zero and $s = s' = 0$. Note that a factor of $1/2$ is put into the present definition of the kernel which is not present in the functions displayed in references 1 and 2. The singularity that occurs when the arc length or fillet radius is zero and $s = s' = 0$ is illustrated in reference 1. The function, $K_{III}*(s, s')$, for $r_s = 0$, is not bounded throughout the entire region of integration but, rather, increases indefinitely as one approaches the origin along an arbitrary line, $s/s' = $ constant. However, the value of the function, $G(s)$, at the inner corner of the adjoint plates is finite and is determined with the aid of a Liouville-Neumann expansion in powers of the parameter, λ. The sum of this series is a simple formula which was found and exploited to great advantage in reference 1. For the two examples elaborated here $G(0)$ yields

$$\frac{Q(0)}{\sigma T_0^4} = \frac{\epsilon}{1 + \epsilon} \tag{26}$$

and

$$\frac{\sigma T^4(0)}{Q_0} = \frac{1 + \epsilon}{\epsilon} \tag{27}$$

These formulas are of considerable value in tying down the numerical solution in a region where the computed data begin to scatter, that is, near $s = s' = 0$ for $r_s = 0$.

Another special situation, not involving a singularity of the kernel, arises when $r_s = 1$. Here $K(s, s')$ reduces to $K_I(s, s')$, the inversion of equation (12) is possible, as shown in reference 2, and formulas (17) and (18) result.

PRESENTATION OF RESULTS

Two problems of physical interest have been formulated so that they emerge directly from equation (4) when a transformation, equation (8), is made. The transformation casts (4) into a form containing the two functions, $Q(s)$ and $\sigma T^4(s)$, explicitly. When either function is regarded as a given constant of the problem, the basic equation for the other function reduces to equation (10) or (11). It is only for convenience in presentation, however, that one function is regarded as a constant. The machine program developed to handle equation (9) and applied to (10) and (11) is equally valid when an arbitrary boundary condition is given. To facilitate the presentation of the numerical results that illustrate the effect of a fillet, however, it suffices to use a constant, either T_O or Q_O, as the prescribed function on the boundary. Solutions to the integral equations, (10) and (11), discussed here may be found in figures 5 and 6, respectively. The emissivity and fillet size appear as parameters.

Figure 5, a graph of $Q(s)/\sigma T_O^4$ versus s, consists of three groups of curves: an upper group, middle group, and lower group, illustrating the level of variation for three representative values of the emissivity, namely, $\epsilon = 0.9, 0.5$, and 0.1. Each curve within a group depicts the actual behavior of the function. Several values of fillet size are plotted, including the two limiting cases, $r_S = 0$ and $r_S = 1.0$.

It is evident from figure 5 that, for a given surface temperature, T_O, the heat-transfer distribution, $Q(s)/\sigma T_O^4$, is affected in two ways. First, for any value of emissivity the distribution for the unfilleted structure tends toward uniformity when a fillet is added. The spread between maximum and minimum heat-transfer values of any curve diminishes with increasing fillet size. The greatest spread occurs for the unfilleted structure whereas the circular arc ($r_S = 1$) sustains the least variation of heat transfer along its surface. Second, for a given fillet size the level of the variation of the heat transfer diminishes with decreasing emissivity. As one might expect, therefore, a fillet has the greatest effect for surfaces with high emissivities. The influence on surfaces with low emissivities is small.

Figure 6 presents the temperature distribution on a filleted structure with constant heat transfer. The scale constant, Θ_O, that appears on the figure is the value of the function $\sigma T^4(0)/Q_O$ at $s = 0$ for $r_S = 1$ and for a given ϵ (eq. (18)); it is presented as figure 6(a). As ϵ decreases Θ_O increases and the curve is arbitrarily terminated at $\epsilon = 0.01$ as a practical limit. The temperature function $\sigma T^4(s)/Q_O - \Theta_O$ is given in figure 6(b) along with three dashed curves. The latter curves are typical results based upon the use of an approximation which introduces a shape factor. A discussion of the approximation is given in the next section.

It can be seen from the results in figure 6(b) that for a given heat transfer, Q_O, to the surface, the temperature distribution, $\sigma T^4(s)/Q_O$, is affected only by the fillet size and not by the surface emissivity, a consequence of the transformation that was found, namely, equation (14). The maximum temperature occurs at the corner of the unfilleted structure but this temperature is reduced and occurs at the juncture of the two surfaces when a fillet is introduced. For

a fixed value of emissivity the spread between maximum and minimum temperatures diminishes with increasing fillet size. The greatest spread occurs for the unfilleted structure whereas the circular arc, as before, sustains the least variation in temperature along its surface. In this case, however, the gradient along the surface is independent of emissivity. It should be noted though, that the temperature variation along the surface becomes less and less significant as the emissivity is reduced since the spread in temperatures becomes a smaller and smaller fraction of the maximum temperature of the surface. Thus, as with the previous example, the influence of the fillet is reduced with decreasing emissivity.

For the range of parameters explored in this presentation only small values of ϵ cause convergence difficulty. A method of accelerating convergence was developed in reference 1 and is contained in the machine program used here. Two other parameters that have not been mentioned so far but appear in the machine program are the step size and the desired accuracy of the computed result. A total of 51 equispaced field points on the surface at which a value of a function is calculated are used. This is a step size of 0.02 since the total surface length, L_T, is set equal to 1 in the machine code but equals 2 in the formulation of the problem and the presentation of computed results. A finer step size, 0.01, did not alter any numerical results, to four significant figures, except when very near the origin for small fillet sizes. Some variation in the third significant figure then is observed but little difficulty is experienced in fairing curves because the value at the origin is known. The iteration procedure, for all computed results, was continued until the difference in successive iterates was less than 0.0001.

The value of either function, $Q(s)/\sigma T_o^4$ or $\sigma T^4(s)/Q_o$, at the juncture of the fillet and plane surfaces is obtained by extrapolation of the curves on either side of the juncture point. This is necessary inasmuch as the juncture point is not one of the equispaced field points. Except for fillet sizes less than triple the step size, that is, 0.06, this is satisfactory because there are then three points through which the curve can be constructed. However, it is not necessary to use a finer step to obtain the curve corresponding to fillets less than 0.06 because the value of the function is known at the point of symmetry, $s = 0$, and the value at the junction can be obtained by extrapolating only the solution from the right. The ordinates of the intersection of this extrapolated curve and the ordinate, $s = r_S$, is the desired value. These two values provided an upper and lower bound on the cosine function which corresponds to the fillet portion of the surface. The slope of this function is zero at $s = 0$ and there is enough information, in most instances, to estimate adequately the curve between $s = 0$ and $s = r_S$. In the two figures, 5 and 6(b), curves for $r_S = 0.01$ and 0.05 are drawn in this way.

The code that was developed by H. Lomax for equation (9) with kernel function, equation (21), differs from that discussed in reference 1 in the manner in which the configuration and composite kernel are introduced. Also it was unnecessary to incorporate into the program the analytic formula to replace the corner singularity. However, the iterative scheme and convergence tests are the

12

same and the reader may consult this reference concerning these two aspects of the numerical method as well as a discussion of the technique by which the rate of convergence can be accelerated.

It is interesting to consider an alternate presentation of the solutions to equations (10) and (11) which define two distinct physical problems. Instead, one might begin with a mathematical problem defined by equation (12), the Fredholm integral equation of the second kind with symmetric kernel. The kernel is characterized by the parameter, r_s, as before. The solutions to this equation can be represented by a two-parameter family of curves, $G(s)$, the parameters being λ and r_s instead of ϵ and r_s. An example of this family is given by figure 6(b) when $\epsilon = 1.0$. This group of curves represents, in the mathematical sense, the variation of $G(s)$ with s for $\lambda = 1.0$ and several values of the kernel parameter, r_s. The envelope of the solutions shown in this figure is defined by the curves corresponding to $r_s = 0$ and $r_s = 1.0$. As the parameter λ is reduced from 1 to 0, the size of the envelope as well as the level of the entire group of curves is also reduced. In the limit that $\lambda = 0$, the envelope coalesces to the single curve, $G(s) = 1.0$. The transformations, equations (13) and (14), lead from the mathematical problem as stated above back to the two physical problems which have been discussed previously and whose solutions are given in figures 5 and 6.

APPROXIMATION USING SHAPE FACTOR

An approximate solution, $G_1(s)$, of the canonical form of the radiation integral equation, equation (12), is obtained under the assumption that the variation of $G(s')$ with s' can be ignored with respect to the variation of $K(s, s')$ with s'. It is possible, therefore, to replace $G(s')$ by $G(s)$ and the resultant expression is

$$G_1(s) = \frac{1}{1 - \lambda f(s)} \tag{28}$$

where $f(s)$, called the shape factor, is

$$f(s) = \int_{L_T} K(s, s')ds' \tag{29}$$

or alternately

$$f(s) = 1 - \frac{1}{2}\left[\sin \varphi(s, -1) - \sin \varphi(s, +1)\right], \quad s \geq 0 \tag{30}$$

and

$$\left|\sin \varphi(s, s')\right| = \frac{a}{c} \tag{31}$$

See, for example, figure 1. Equation (30) is especially convenient to graphical determination of the shape factor.

13

For comparison with the exact numerical solution of equations (10) and (11), the corresponding approximate solutions are

$$\frac{Q_1(s)}{\sigma T_0{}^4} = \frac{[\epsilon\, 1 - f(s)]}{1 - (1 - \epsilon)f(s)} \tag{32}$$

and

$$\frac{\sigma T_1{}^4(s)}{Q_0} = \frac{1}{\epsilon} + \frac{f(s)}{1 - f(s)} \tag{33}$$

As a measure of accuracy of the approximation, the quantities

$$\frac{Q(s) - Q_1(s)}{Q_R} \tag{34}$$

and

$$\frac{\sigma T^4(s) - \sigma T_1{}^4(s)}{\sigma T_R{}^4} \tag{35}$$

were computed for a representative number of points and for the same values of the two parameters illustrated in figures 5 and 6(b). For these values of the two parameters, the absolute value of (34) is found to be less than 0.09 and the absolute value of (35) is found to be less than 0.05 everywhere.

In both physical problems considered, the greatest disagreement between exact and approximate solutions occurs for a fillet size of about 0.1. The dependence of expressions (34) and (35) on emissivity, in contrast to their dependence on fillet size, differs for the two cases. For the constant temperature case, expression (34) increases with decreasing emissivity, being 0.006 for $\epsilon = 0.9$, whereas it is 0.09 for $\epsilon = 0.1$. For the constant heat-transfer case, expression (35) decreases with decreasing emissivity. An emissivity, $\epsilon = 0.9$, yields the value 0.05 for expression (35) but when $\epsilon = 0.1$, the same expression yields a value of 0.009. These results suggest also that in the mathematical sense the approximation, $G_1(s)$, most accurately represents the exact value $G(s)$, given by equation (12), for low values of λ where $0 \leq \lambda \leq 1$. Approximate results, shown as dashed lines on figure 6(b), are presented only for the constant heat-transfer case because this case represents a significant departure of the approximate solution from the exact solution and at the same time the largest variation in the function $\sigma T^4(s)/Q_0$. The constant temperature example for high values of ϵ in which the variation of $Q(s)/T_0{}^4$ is significant is well represented by the formula, equation (34).

At the corner, $s = 0$, for all values of emissivity and for $r_s = 0$, the approximation $G_1(s)$ is seen to yield exact results; that is, equations (30) and (32), and (30) and (33) lead to equations (26) and (27), respectively, since $f(0) = 1/2$ for $r_s = 0$. This explains, in part, why a maximum is observed in expressions (34) and (35) when they are regarded as continuous functions of r_s.

14

Without the corner formulas, (26) and (27), the available numerical data used in equation (29) and, hence, the approximate solutions, (32) and (33), do not suggest such a maximum. The approximation appears to break down whereas it is actually exact at the corner.

Ames Research Center
    National Aeronautics and Space Administration
        Moffett Field, Calif., Sept. 24, 1962.

REFERENCES

1. Heaslet, Max. A., and Lomax, Harvard: Numercial Predictions of Radiative Interchange Between Conducting Fins With Mutual Irradiations. NASA TR R-116, 1961.

2. Heaslet, Max. A., and Lomax, Harvard: Radiative Heat-Transfer Calculations for Infinite Shells With Circular-Arc Sections, Including Effects of an External Source Field. International Journal of Heat and Mass Transfer, Vol. 5, June, 1962, pp. 457-468.

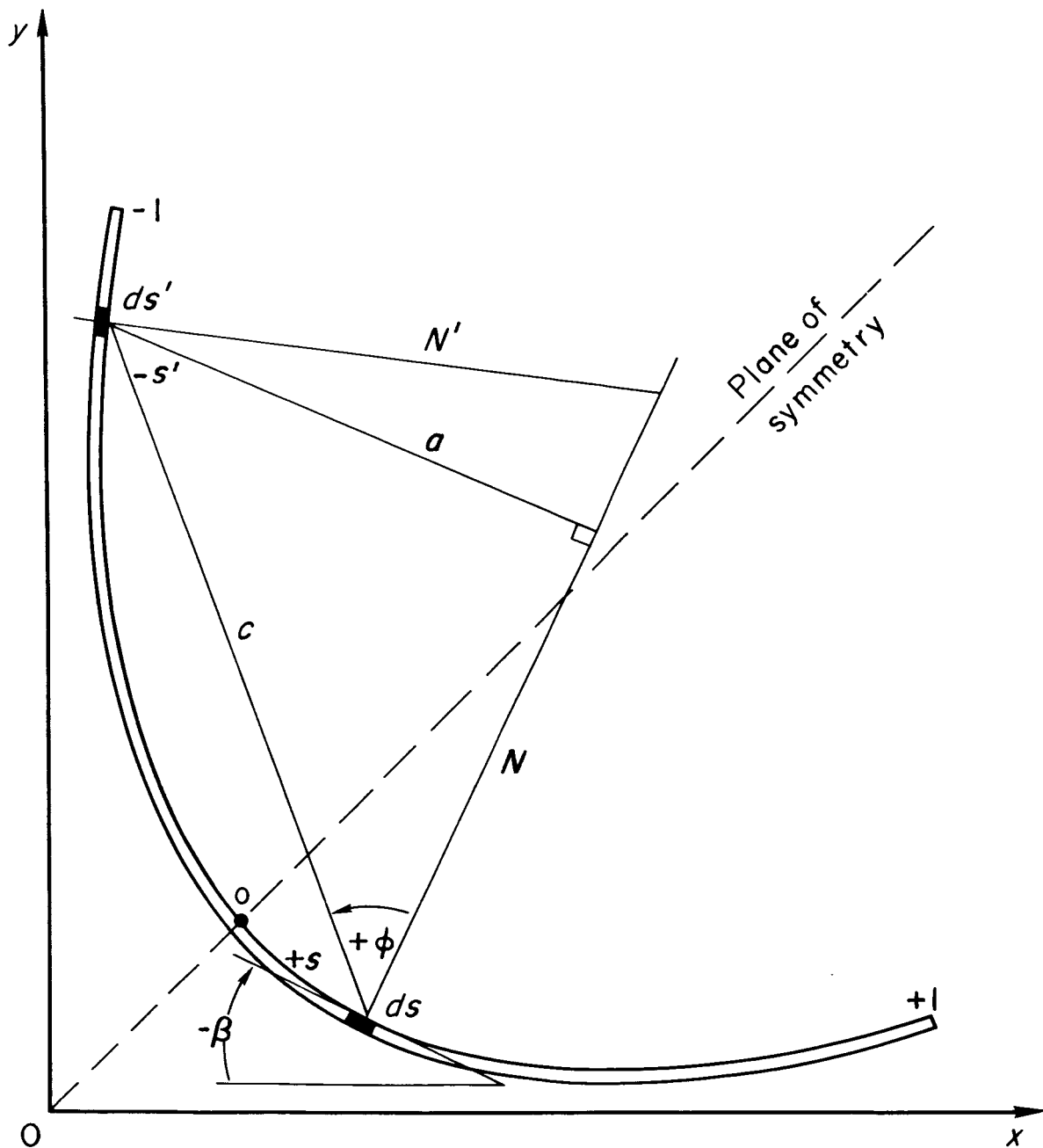3. Jakob, Max: Heat Transfer, Vol. 2, John Wiley and Sons, New York, 1957, pp. 19-21.

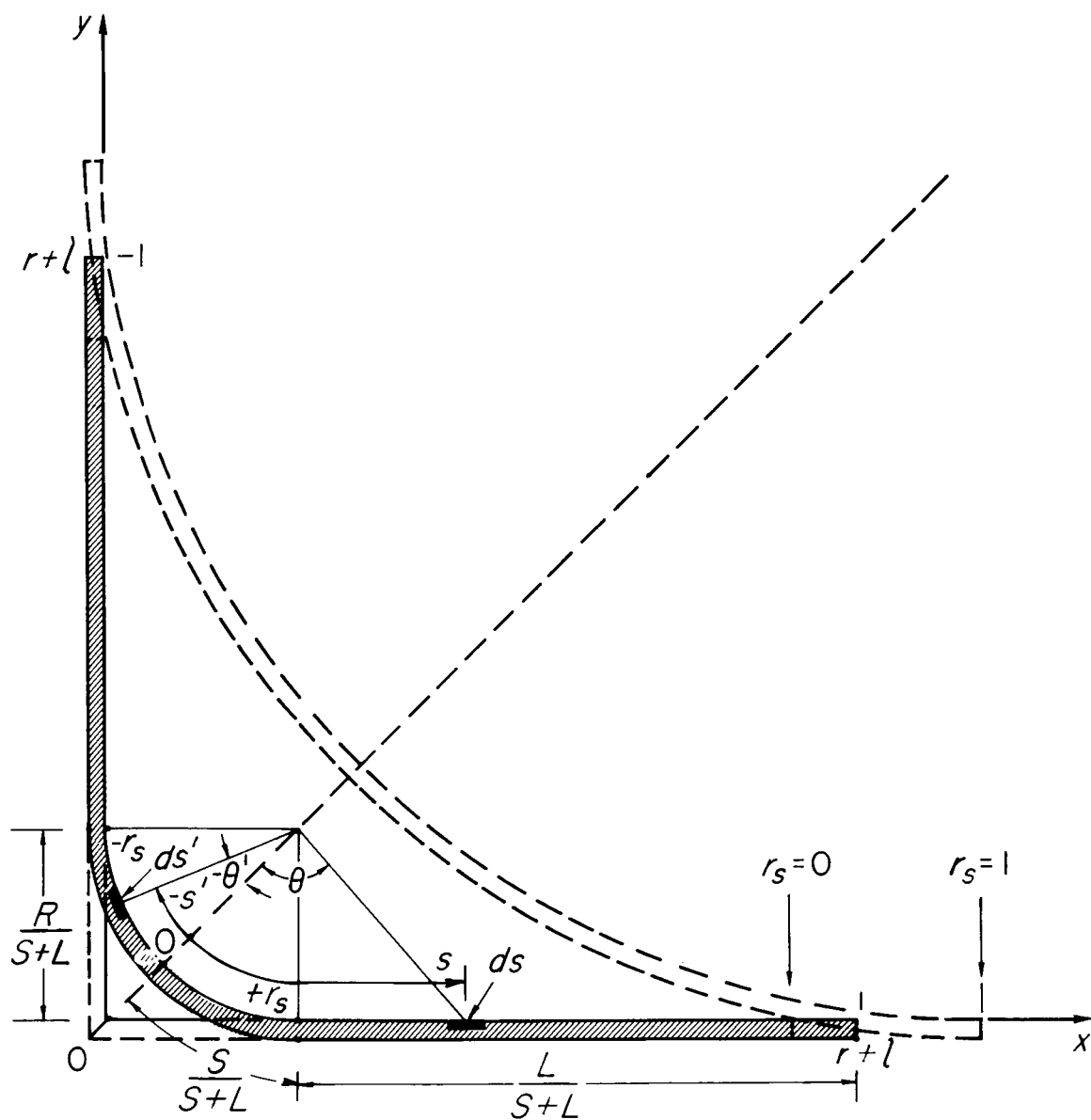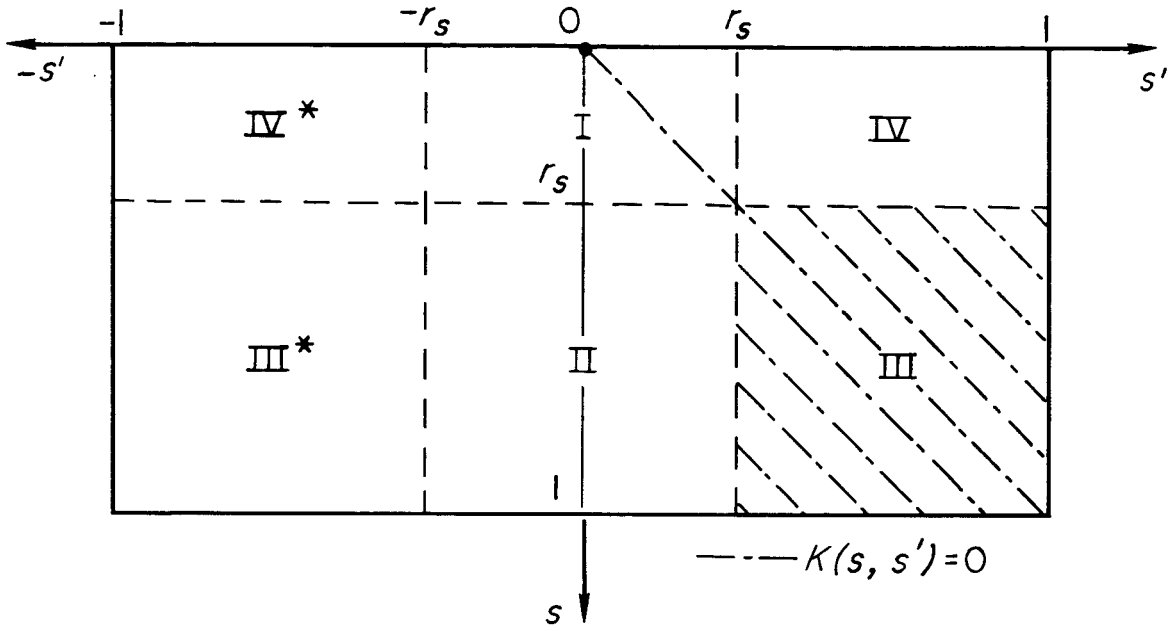Figure 1.- Two-dimensional section of a surface radiating diffusely from the concave side.

Figure 2.- Coordinates of composite surface with three values of the parameter, $r_s = S/(S + L)$, shown.

$$K_I(s, s') = \frac{\pi}{16r_s} \sin\left(\frac{\pi}{8r_s}|s - s'|\right)$$

$$K_{II}(s, s') = \frac{\pi}{8r_s}\left[1 - \cos\frac{\pi}{4}\left(1 - \frac{s'}{r_s}\right)\right] \frac{\left[1 - \cos\frac{\pi}{4}\left(1 - \frac{s'}{r_s}\right) + \frac{\pi}{4}\left(\frac{s}{r_s} - 1\right)\sin\frac{\pi}{4}\left(1 - \frac{s'}{r_s}\right)\right]}{\left\{2\left[1 - \cos\frac{\pi}{4}\left(1 - \frac{s'}{r_s}\right) + \frac{\pi}{4}\left(\frac{s}{r_s} - 1\right)\sin\frac{\pi}{4}\left(1 - \frac{s'}{r_s}\right)\right] + \left[\frac{\pi}{4}\left(\frac{s}{r_s} - 1\right)\right]^2\right\}^{3/2}}$$

$$K_{III}(s, s') = 0$$

$$K_{III*}(s, s') = \frac{\pi}{8r_s} \frac{\left[1 + \frac{\pi}{4}\left(\frac{s}{r_s} - 1\right)\right]\left[1 + \frac{\pi}{4}\left(-\frac{s'}{r_s} - 1\right)\right]}{\left\{\left[1 + \frac{\pi}{4}\left(\frac{s}{r_s} - 1\right)\right]^2 + \left[1 + \frac{\pi}{4}\left(-\frac{s'}{r_s} - 1\right)\right]^2\right\}^{3/2}}$$

$$K_{IV}(s, s') = \frac{\pi}{8r_s}\left[1 - \cos\frac{\pi}{4}\left(1 - \frac{s}{r_s}\right)\right] \frac{\left[1 - \cos\frac{\pi}{4}\left(1 - \frac{s}{r_s}\right) + \frac{\pi}{4}\left(\frac{s'}{r_s} - 1\right)\sin\frac{\pi}{4}\left(1 - \frac{s}{r_s}\right)\right]}{\left\{2\left[1 - \cos\frac{\pi}{4}\left(1 - \frac{s}{r_s}\right) + \frac{\pi}{4}\left(\frac{s'}{r_s} - 1\right)\sin\frac{\pi}{4}\left(1 - \frac{s}{r_s}\right)\right] + \left[\frac{\pi}{4}\left(\frac{s'}{r_s} - 1\right)\right]^2\right\}^{3/2}}$$

$$K_{IV*}(s, s') = \frac{\pi}{8r_s}\left[1 - \sin\frac{\pi}{4}\left(1 - \frac{s}{r_s}\right)\right] \frac{\left[1 - \sin\frac{\pi}{4}\left(1 - \frac{s}{r_s}\right) + \frac{\pi}{4}\left(-\frac{s'}{r_s} - 1\right)\cos\frac{\pi}{4}\left(1 - \frac{s}{r_s}\right)\right]}{\left\{2\left[1 - \sin\frac{\pi}{4}\left(1 - \frac{s}{r_s}\right) + \frac{\pi}{4}\left(-\frac{s'}{r_s} - 1\right)\cos\frac{\pi}{4}\left(1 - \frac{s}{r_s}\right)\right] + \left[\frac{\pi}{4}\left(\frac{-s'}{r_s} - 1\right)\right]^2\right\}^{3/2}}$$

Figure 3.- Kernel function in surface coordinates listed according to relative location of field (s) and source (s') points.

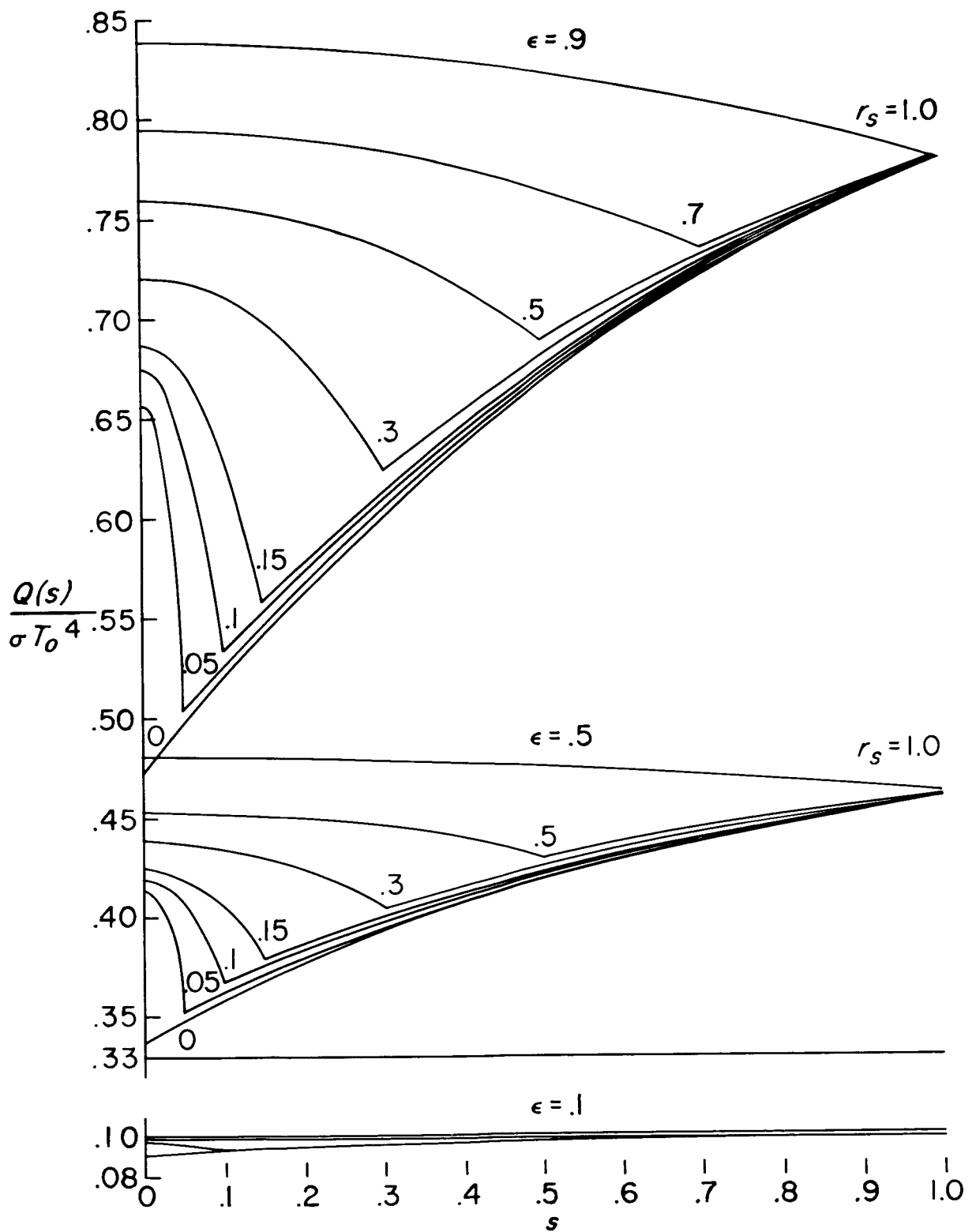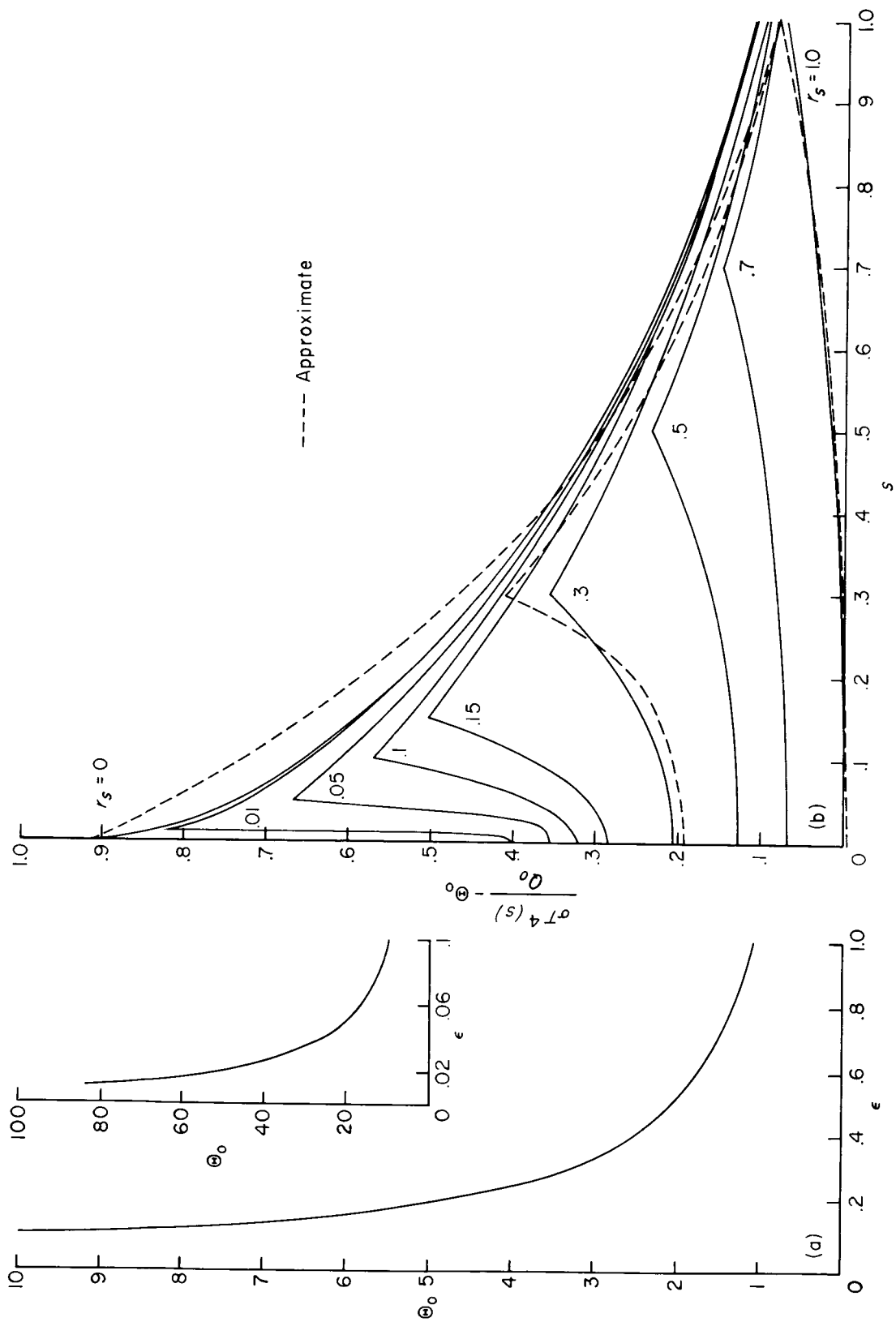Figure 4.- Kernel function in radiation integral equation ($r_s = 0.3$).

Figure 5.- Local heat-transfer variation for uniform temperature.

(a) Scale constant.

(b) Temperature function.

Figure 6.- Temperature variation for constant heat transfer with associated scale constant.